

Linear Stability of a Developing Thermal Front Induced by a Constant Heat Flux

Aminreza Noghrehabadi · D. Andrew S. Rees · Andrew P. Bassom

Received: 24 February 2013 / Accepted: 11 June 2013 / Published online: 17 July 2013
© Springer Science+Business Media Dordrecht 2013

Abstract A developing thermal front is set up by suddenly imposing a constant heat flux on the lower horizontal boundary of a semi-infinite fluid-saturated porous domain. The critical time for the onset of convection is determined using two main forms of analysis. The first of these is an approximate method which is effectively a frozen-time model while the second implements a set of parabolic simulations of monochromatic disturbances placed in the boundary layer at an early time. Results from the two approaches are compared and it is found that instability only occurs when the nondimensional disturbance wavenumber, k , is less than unity. The neutral curve for the primary mode possesses a vertical asymptote at $k = 1$ in wavenumber/time parameter space which is in contrast to the more usual teardrop shape which occurs when the surface is subject to a constant temperature. Asymptotic analyses are performed for the frozen-time model which yield excellent predictions for both branches of the neutral curve and the locus of the maximum growth rate curve at late times.

Keywords Convective instabilities · Linear theory · Porous medium · Boundary layer · Thermal front · Constant heat flux

List of Symbols

A_1, A_2	Disturbance amplitude measures
c.c.	Complex conjugate
g	Gravity

A. Noghrehabadi
Department of Mechanical Engineering, Shahid Chamran University of Ahvaz, Ahvaz, Iran
e-mail: a.r.noghrehabadi@scu.ac.ir

D. A. S. Rees (✉)
Department of Mechanical Engineering, University of Bath, Bath BA2 7AY, UK
e-mail: d.a.s.rees@bath.ac.uk

A. P. Bassom
School of Mathematics and Statistics, University of Western Australia, Crawley, WA 6009, Australia
e-mail: andrew.bassom@uwa.edu.au

k	Wavenumber of disturbance
k_{pm}	Conductivity of the porous medium
K	Permeability
L	Natural length scale
q''	Surface rate of heat flux
p	Pressure
Ra	Darcy-Rayleigh number
t	Time
T	Dimensional temperature
u	Horizontal velocity
v	Vertical velocity
x	Horizontal coordinate
y	Vertical coordinate
Z_0	The first zero of the Airy function (-2.338107)

Greek Characters

α	Thermal diffusivity
β	Expansion coefficient
δ	Amplitude of disturbance
η	Similarity variable
θ	Nondimensional temperature
Θ	Disturbance temperature
λ	Exponential growth rate
μ	Dynamic viscosity
ρ	Density
σ	Heat capacity ratio
τ	Scaled time
τ_0	Initiation time
ψ	Streamfunction
Ψ	Disturbance streamfunction

Superscripts and Subscripts

0, 1, 2, 3	Terms in asymptotic series
∞	Ambient/initial conditions
-	Dimensional quantities
'	Derivative with respect to η
^	Sublayer terms in Appendix 2
~	Sublayer terms in Appendix 3
b	Basic state
bl	Associated with the boundary layer thickness
c	Critical conditions
loc	Local
max	Maximum
τ	Derivative with respect to τ

1 Introduction

This paper considers the initial destabilisation of a diffusing thermal front in a saturated porous medium. The front is caused by the sudden heating of the lower boundary of a semi-infinite medium by means of a constant heat flux; subject to certain conditions being satisfied, this configuration is identical with the case of the upper boundary of a porous medium being subject to a constant flux of solute, where it is assumed that the dissolved solute is more dense than the ambient fluid.

There now exists a sizeable body of research on this type of topic, which is characterised by an unsteady but nonperiodic basic state. A fairly recent review may be found in [Rees et al. \(2008b\)](#) where, among other aspects, much space was devoted to a comparison between different methods of solution for the linearised disturbance equation. There are four main methods: (i) a local Rayleigh number analysis, where stability criteria drawn from a relatively straightforward configuration, such as the Darcy-Bénard problem, are applied to the unsteady problem in order to gain a rough idea of the latter's stability properties; (ii) a quasi-steady-state approximation (QSSA), wherein the time derivative is set to zero in order to obtain an ordinary differential eigenvalue problem for the critical time and wavenumber; (iii) an energy analysis based on the behaviour of energy functionals; and (iv) a numerical simulation of the full linearised stability equations which are parabolic in time.

Most of the analyses to date on the instability of unsteady boundary layers are equivalent to cases of heating from below using a constant temperature boundary condition. We also note that many studies deal with a finite layer, but the semi-infinite domain which forms the present interest is equivalent to situations in which the Darcy-Rayleigh number based upon the height of the layer is large, and these are known as a deep pool system.

One of the earliest studies was the nonlinear simulations of [Elder \(1967, 1968\)](#), where the heated surface was also subject to random perturbations in order to initiate disturbances in the bulk. [Caltagirone \(1980\)](#) employed an energy analysis to obtain stability criteria, and he supplemented this with some further nonlinear simulations. Later, [Yoon and Choi \(1989\)](#) and [Kim et al. \(2002\)](#) presented linear analyses which adopt the QSSA, although the basic state, which takes the form of a complementary error function, was approximated by a fourth order polynomial. The QSSA effectively assumes that two timescales operate independently, namely the those of the disturbance (which is fast) and that of the basic state (which is slow). Although numerical simulations of the full linearised disturbance equations show that there is no such distinction, the results obtained this way are nevertheless moderately accurate.

[Selim and Rees \(2007a\)](#) undertook numerical simulations of the fully parabolic disturbance equations in order to construct a neutral stability curve. Much of their discussion centred on whether it is possible to define neutral stability unambiguously, and to that end they evaluated different measures for the amplitude of the evolving disturbance. Measures such as the heat transfer at the bounding surface, the maximum temperature of the disturbance, and an energy integral, were considered, and each gave a different stability curve, the last of the three forming the lowest curve. They also showed that such neutral curves are essentially independent of the shape of the initiating disturbance, but only when it is imposed well before the onset time. While this latter point could be seen as significant, we also note that it does not always apply in general: see the analysis of the stability of a line source plume given in [Rees et al. \(2008\)](#).

The identity of the most unstable disturbance has also been the subject of enquiry. [Rapaka et al. \(2008\)](#) used a technique based upon singular value decomposition to identify not only the most unstable disturbance at any chosen point in time, but also the initial condition that would lead to that disturbance shape. While such a technique will undoubtedly minimise the critical time, in practice any naturally occurring heterogeneities are unlikely to take the form

of that pure profile, and therefore these results could represent an essentially unattainable onset time.

Other papers of note include that of [Wessel-Berg \(2009\)](#) which solves essentially the same problem as [Selim and Rees \(2007a\)](#) where the solution is based upon Hermite polynomials which are associated with the disturbance equation for the solute at early times. The effect of local thermal nonequilibrium was studied in detail by [Nouri-Borujerdi et al. \(2007\)](#). A linearly increasing lower temperature was studied by [Hong et al. \(2008\)](#) who compared the results of a QSSA and a local Rayleigh number analysis. [Hidalgo and Carrera \(2009\)](#) considered the additional effect of dispersion, and extrapolated onset times from detailed nonlinear simulations. [Hassanzadeh et al. \(2009\)](#) also considered dispersion, but combined it with the presence of horizontal flow to mimic injection into an aquifer. [Nield and Kuznetsov \(2010\)](#) and [Kuznetsov et al. \(2011\)](#) have considered the effect of heterogeneous media on the onset of convection; they looked at heating from below for both a sudden rise in temperature and a sudden change in heat flux. The interaction with chemical reactions, as might be experienced during carbon capture and sequestration, was analysed by [Ennis-King and Paterson \(2007\)](#). Finally, nonlinear simulations covering a wide variety of aspects include those of [Tan et al. \(2003\)](#), [Riaz et al. \(2006\)](#), [Selim and Rees \(2007b, 2010a,b\)](#), [Hassanzadeh et al. \(2007\)](#) and [Rapaka et al. \(2008\)](#).

Despite the wealth of papers on this general topic, very few have considered sudden heating using a constant heat flux. While a few of those quoted above do indeed provide some information, it is quite astonishing that a comprehensive analysis is still lacking. For example, [Kim et al. \(2004\)](#) provide a QSSA analysis and quote a critical modified Rayleigh number (equivalent to a dimensionless time) and the associated wavenumber. The present paper, therefore, is devoted to a very detailed analysis of the neutral curves for this system. We will present a brief local Rayleigh number analysis, a QSSA analysis (together with an asymptotic analysis of the behaviour of the right-hand branch of the neutral curve) and parabolic simulations. Indeed, we find that the right-hand branch has an unusual characteristic, namely that the wavenumber tends towards a constant value as time progresses, unlike its constant temperature analogue where the wavenumber tends towards zero.

2 Governing Equations and Basic Solution

We consider the onset of convection in an initially quiescent semi-infinite region of saturated porous medium ($0 \leq \bar{y} < \infty$, $-\infty < \bar{x} < \infty$) which has been held at the uniform temperature, T_∞ , where the lower boundary ($\bar{y} = 0$) is suddenly subjected to heating by means of a constant rate of heat flux at $t = 0$ and at all times thereafter. The porous medium is assumed to be homogeneous and isotropic, and it is also assumed that the flow is governed by Darcy's law modified by the presence of buoyancy and subject to the Boussinesq approximation. The fluid and the porous matrix are also assumed to be in local thermal equilibrium when considering the thermal energy equation. We will consider two-dimensional perturbations because the linearised disturbance equations may always be Fourier-decomposed into two-dimensional components of the form we consider here. Given these observations and assumptions, the governing equations of motion and for the temperature field may be written as follows,

$$\frac{\partial \bar{u}}{\partial \bar{x}} + \frac{\partial \bar{v}}{\partial \bar{y}} = 0, \quad (1)$$

$$\bar{u} = -\frac{K}{\mu} \frac{\partial \bar{p}}{\partial \bar{x}}, \quad (2)$$

$$\bar{v} = -\frac{K}{\mu} \frac{\partial \bar{p}}{\partial \bar{y}} + \frac{\rho g \beta K}{\mu} (T - T_\infty), \tag{3}$$

$$\sigma \frac{\partial T}{\partial \bar{t}} + \bar{u} \frac{\partial T}{\partial \bar{x}} + \bar{v} \frac{\partial T}{\partial \bar{y}} = \alpha \left(\frac{\partial^2 T}{\partial \bar{x}^2} + \frac{\partial^2 T}{\partial \bar{y}^2} \right). \tag{4}$$

In these equations \bar{x} and \bar{y} are the respective Cartesian coordinates in the horizontal and vertical directions while the corresponding velocities are \bar{u} and \bar{v} . All the other terms have their usual meaning for porous medium convection and are given in the List of Symbols. The heated horizontal surface is held at the uniform rate of heat flux,

$$-k_{pm} \frac{\partial T}{\partial \bar{y}} \Big|_{\bar{y}=0} = q''. \tag{5}$$

A Darcy-Rayleigh number may be defined as follows,

$$Ra = \frac{\rho g \beta K L^2 q''}{\mu \alpha k_{pm}}, \tag{6}$$

where L is a lengthscale. Given that there is no naturally-occurring lengthscale in the system which we are considering, it is reasonable to define one in terms of the properties of the porous medium and the fluid:

$$L = \left(\frac{\mu \alpha k_{pm}}{\rho g \beta K q''} \right)^{1/2}. \tag{7}$$

This value of L is equivalent to setting $Ra = 1$ in Eq. (6)

Equations (1)–(4) may now be nondimensionalised using the following transformations,

$$\bar{t} = \frac{\sigma L^2}{\alpha} t, \quad (\bar{x}, \bar{y}) = L(x, y), \quad (\bar{u}, \bar{v}) = \frac{\alpha}{L}(u, v), \quad \bar{p} = \frac{\alpha \mu}{K} p, \quad T = T_\infty + \frac{q'' L}{k_{pm}} \theta, \tag{8}$$

and they yield the following set of dimensionless governing equations:

$$\frac{\partial u}{\partial x} + \frac{\partial v}{\partial y} = 0, \tag{9}$$

$$u = -\frac{\partial p}{\partial x}, \tag{10}$$

$$v = -\frac{\partial p}{\partial y} + \theta, \tag{11}$$

$$\frac{\partial \theta}{\partial t} + u \frac{\partial \theta}{\partial x} + v \frac{\partial \theta}{\partial y} = \frac{\partial^2 \theta}{\partial x^2} + \frac{\partial^2 \theta}{\partial y^2}. \tag{12}$$

The appropriate boundary conditions are:

$$y = 0: \quad v = 0, \quad \frac{\partial \theta}{\partial y} = -1 \quad \text{and} \quad y \rightarrow \infty: \quad v, \theta \rightarrow 0, \tag{13}$$

while $\theta = 0$ everywhere for $t < 0$.

The pressure may be eliminated between Eqs. (10) and (11) and the streamfunction, ψ , may now be defined according to,

$$u = -\frac{\partial \psi}{\partial y} \quad \text{and} \quad v = \frac{\partial \psi}{\partial x}, \tag{14}$$

so that the equation of continuity is satisfied. Therefore Eqs. (10)–(12) reduce to the pair,

$$\frac{\partial^2 \psi}{\partial x^2} + \frac{\partial^2 \psi}{\partial y^2} = \frac{\partial \theta}{\partial x}, \tag{15}$$

$$\frac{\partial \theta}{\partial t} + \frac{\partial \psi}{\partial x} \frac{\partial \theta}{\partial y} - \frac{\partial \psi}{\partial y} \frac{\partial \theta}{\partial x} = \frac{\partial^2 \theta}{\partial x^2} + \frac{\partial^2 \theta}{\partial y^2}, \tag{16}$$

which are to be solved subject to the boundary conditions,

$$y = 0: \psi = 0, \quad \frac{\partial \theta}{\partial y} = -1 \quad \text{and} \quad y \rightarrow \infty: \psi, \theta \rightarrow 0, \tag{17}$$

and the initial condition that

$$\psi = \theta = 0 \quad \text{at} \quad t = 0. \tag{18}$$

We note that the setting of ψ to zero at $y = 0$ means that the impermeability condition, $v = \psi_x = 0$ is satisfied. The corresponding boundary condition as $y \rightarrow \infty$ is equivalent both to zero vertical flow far from the surface and an overall zero mean horizontal velocity flux.

The resulting basic profile consists of a motionless state given by $\psi = 0$ and an evolving temperature field which is uniform horizontally. Therefore the heat transport equation for the purely conducting basic state reduces to,

$$\frac{\partial \theta}{\partial t} = \frac{\partial^2 \theta}{\partial y^2}, \tag{19}$$

and the analytical solution is

$$\theta_b = t^{1/2} \left[\frac{2}{\sqrt{\pi}} e^{-\eta^2} - 2\eta \operatorname{erfc}(\eta) \right], \tag{20}$$

where the similarity variable, η , is defined according to,

$$\eta = \frac{y}{2\sqrt{t}}; \tag{21}$$

this and solutions of similar types of sudden heating problem may also be found in [Carslaw and Jaeger \(1959\)](#).

In this paper, we choose to follow the work of [Selim and Rees \(2007a,b, 2010a,b\)](#) and to consider disturbances to the basic profile after first transforming the governing equations into the coordinate system (η, τ) where η is given above, and

$$\tau = \sqrt{t} \tag{22}$$

is the scaled time. The transformation of the time-coordinate removes square root singularities near to $t = 0$. Equations (15)–(16) now become,

$$4\tau^2 \frac{\partial^2 \psi}{\partial x^2} + \frac{\partial^2 \psi}{\partial \eta^2} = 4\tau^2 \frac{\partial \theta}{\partial x}, \tag{23}$$

$$2\tau \frac{\partial \theta}{\partial \tau} + 2\tau \left(\frac{\partial \psi}{\partial x} \frac{\partial \theta}{\partial \eta} - \frac{\partial \psi}{\partial \eta} \frac{\partial \theta}{\partial x} \right) = 4\tau^2 \frac{\partial^2 \theta}{\partial x^2} + \frac{\partial^2 \theta}{\partial \eta^2} + 2\eta \frac{\partial \theta}{\partial \eta}. \tag{24}$$

We note that it is possible to define a local (i.e., an unsteady) Rayleigh number by using the thickness of the evolving thermal field as the lengthscale. Given the form of the above similarity variable, it is clear that such a lengthscale is proportional to $t^{1/2}$ (or τ), and therefore

the local Rayleigh number is proportional to t (or τ^2). Thus the growing thermal boundary layer begins by being stable, becoming unstable when the local Rayleigh number becomes sufficiently large.

3 Local Rayleigh Number Analysis

A crude indication of the critical time and wavenumber may be obtained by comparing the present transient system with that of a horizontal porous layer of uniform thickness which is heated from below with a constant heat flux and cooled above with a constant temperature. [Nield and Bejan \(2006\)](#) give the critical Rayleigh number to be 27.10 and the associated wavenumber as 2.33. For the present system, we may define the following local Rayleigh number which is based upon the growing thickness of the basic thermal boundary layer:

$$Ra_{loc} = \frac{\rho g \beta K q'' \bar{y}_{bl}^2}{\mu \alpha k_{pm}}, \tag{25}$$

where \bar{y}_{bl} is the thickness of the boundary layer. Given that $Ra = \frac{\rho g \beta K L^2 q''}{\mu \alpha k_{pm}} = 1$ by definition, it follows that,

$$Ra_{loc} = \frac{\bar{y}_{bl}^2}{L^2} = y_{bl}^2. \tag{26}$$

We now choose $\eta = 1$ to be the edge of the thermal boundary layer because θ_b has decayed to just less than 10 % of its maximum value at that point. Given that $\eta = y/2\sqrt{t} = y/2\tau$, this means that an alternative form of the local Rayleigh number is,

$$Ra_{loc} = 4t = 4\tau^2. \tag{27}$$

We now set the local Rayleigh number to be equal to that of the corresponding Darcy-Bénard layer:

$$Ra_{loc} = y_{bl}^2 = 4t = 4\tau^2 = 23.10. \tag{28}$$

Therefore we obtain the critical time in the following forms,

$$t = 6.78, \quad \tau = 2.60. \tag{29}$$

For the Darcy-Bénard layer, the nondimensional height of the layer is precisely 1, and the wavelength of the cells is $2\pi/2.33 = 2.697$. Therefore we will assume that the primary mode of convection consists of cells with the same aspect ratio. Given that the boundary layer thickness is now $y_{bl} = 5.21$, the wavelength of cells is $5.21 \times 2.697 = 14.05$, and therefore the predicted wavenumber is

$$k = \frac{2\pi}{14.04} \simeq 0.45. \tag{30}$$

In subsequent sections we will see that the critical time given in Eq. (29) is quite close to what is computed, although the predicted wavenumber is overestimated.

4 Perturbation Analysis

The basic solution as given by $\psi = 0$ and Eq. (20) may now be perturbed in order to determine whether or not the evolving thermal boundary layer is stable. A monochromatic disturbance of asymptotically small magnitude is introduced by setting,

$$\psi(\eta, x, \tau) = \delta \left[i\Psi(\eta, \tau)e^{ikx} + \text{c.c.} \right], \tag{31}$$

$$\theta(\eta, x, \tau) = \theta_b + \delta \left[\Theta(\eta, \tau)e^{ikx} + \text{c.c.} \right], \tag{32}$$

where c.c. denotes complex conjugate and where $|\delta| \ll 1$. Here, the value k is the horizontal wavenumber of the convective roll disturbances. The resulting linearised stability equations are,

$$\Psi'' - 4\tau^2 k^2 \Psi = 4\tau^2 k \Theta, \tag{33}$$

$$2\tau \Theta_\tau = \Theta'' + 2\eta \Theta' - 4\tau^2 k^2 \Theta - 4\tau^2 k \operatorname{erfc}(\eta) \Psi, \tag{34}$$

where primes denote derivatives with respect to η . The boundary conditions are,

$$\eta = 0: \Psi = \frac{\partial \Theta}{\partial \eta} = 0 \quad \text{and} \quad \eta \rightarrow \infty: \Psi, \Theta \rightarrow 0. \tag{35}$$

This system of equations is parabolic in τ and the most natural way in which stability may be assessed is to choose a wavenumber (k), a disturbance initiation time (t_0), and a disturbance profile, and then to monitor how that disturbance evolves with time. However, [Selim and Rees \(2007a\)](#) pointed out that the neutral curve which is obtained by such an analysis depends on precisely how the disturbance amplitude is defined. They employed four different schemes: two based on the surface rate of heat transfer, one on the maximum disturbance temperature and one which is an energy functional, i.e., an integral of the disturbance profile across the boundary layer. Of these schemes, the earliest onset time was given by the functional.

An alternative method is a QSSA wherein the time-derivative in Eq. (34) is neglected, and the system given by Eqs. (33)–(35) is solved as an eigenvalue problem for the critical value of τ as a function of k . The resulting neutral curve is usually qualitatively the same as those obtained by solving the full linear system, but the predicted onset time is substantially later than that given by the energy functional in [Selim and Rees \(2007a\)](#). That this should be so is unsurprising because the setting of $\partial\theta/\partial\tau = 0$ is a strong restriction on the disturbance, one which would not arise in practice unless the initial disturbance profile is specified carefully. We also emphasise the fact that the results of QSSA analysis also depend on whether the zero time derivative is taken before or after the transformation from the (y, t) system to the (η, τ) system; for more discussion, see [Selim and Rees \(2007a\)](#).

5 Neutral Curves

5.1 Quasi-Steady State Analysis

As has already been mentioned, Eqs. (33) and (34) have a single τ -derivative which implies that the linear development of disturbances to the basic flow is governed by a parabolic system. While the streamfunction, Ψ , reacts immediately to changes in Θ , Θ itself varies according to Eq. (34). Therefore one natural way of analysing instability must be to introduce a disturbance into the boundary layer at some point in time and to monitor its evolution with τ

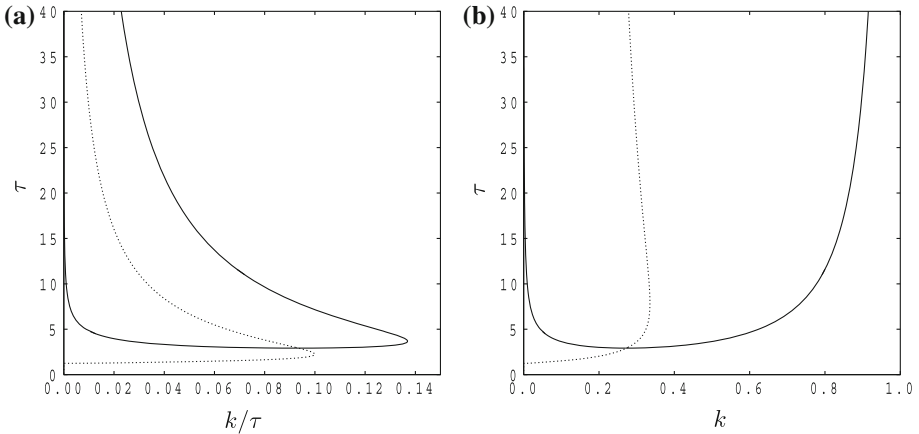


Fig. 1 Neutral curves showing the variation of τ with **a** k/τ and **b** k . The *dotted line* shows the locus of the maximum growth rate for each value of τ

in an appropriate way. However, as a guide to what to expect from such a simulation, we will obtain a reference neutral curve by neglecting the τ -derivative in Eq. (34); this is the essence of a QSSA. Consequently Eqs. (33) and (34) reduce to an ordinary differential eigenvalue problem for the scaled critical time, τ . This approximate system is given by

$$\Psi'' - 4\tau^2 k^2 \Psi = 4\tau^2 k \Theta, \tag{36}$$

$$\Theta'' + 2\eta \Theta' - 4\tau^2 k^2 \Theta - 4\tau^2 k \operatorname{erfc}(\eta) \Psi = 0, \tag{37}$$

which is to be solved subject to the boundary conditions given in Eq. (35). However, since these boundary conditions are homogeneous, it is essential to force a nonzero solution by setting $\Theta(0) = 1$, for example. This extra boundary condition requires an extra equation, and it is given by

$$\tau' = 0, \tag{38}$$

where τ is now regarded as an eigenvalue to be found.

A standard Keller-box method (Keller and Cebeci 1971) was used to solve this eigen-system. In brief, Eqs. (36) and (37), together with either $\tau' = 0$ or $k' = 0$, are reduced to five first-order equations and discretised using second order accurate central differences. The usual marching variable in the Keller box scheme is now either k or τ , so that τ or k , respectively, may be found. We note that the Fréchet derivative, which is a block tridiagonal matrix, is computed within the code rather than specified exactly; this has no effect on the accuracy of the solutions, but code development time is reduced very substantially. In our computations we used a uniform grid of up to 1,601 points in the maximal range $0 \leq \eta < 10$. Larger values of τ generally require smaller domains, but in all cases our computations are correct to at least five significant figures. The results of these computations yield the neutral curves which are shown in Fig. 1a, b.

Figure 1a shows the variation of τ with k/τ and it has the standard single-minimum curve which is typical of very many thermoconvective instabilities. The abscissa, k/τ , may be regarded as being a wavenumber relative to the developing thickness of the basic thermal boundary layer which is proportional to τ . The curve also takes the very familiar tear-drop form which is almost always associated with boundary layer instabilities. In a different

computation we have determined that the critical time and its associated wavenumber, which is the minimum point on the curve displayed in Fig. 1a, are given by

$$\tau_c = 2.922\ 192 \ (t_c = 8.538\ 205), \quad k_c = 0.272\ 965, \quad \tau_c k_c = 0.797656. \quad (39)$$

These values were obtained by solving Eqs. (36) and (37) augmented by the system obtained by differentiating both Eqs. (36) and (37) with respect to k and by setting $\partial\tau/\partial k = 0$. In this case, a fourth-order Runge–Kutta scheme was used together with a standard shooting method for this two-point boundary value problem. The given data are correct to the displayed six decimal places, and they compare well with those of Kim et al. (2004):

$$\tau_c = 2.92 \ (t_c = 8.54), \quad k_c = 0.27, \quad \tau_c k_c = 0.80. \quad (40)$$

The value, $\tau_c k_c$, is termed as a local wavenumber in Kim et al. (2004).

Given that k is fixed for any chosen monochromatic disturbance, the variation of τ with k is shown in Fig. 1b. In this figure those points which are below and to the right of the neutral curve correspond to stability, while instability corresponds to points inside the curve.

In both parts of Fig. 1, we also display the locus of points with the largest growth rate for any point in time. This is an approximate curve because we have set both Ψ and Θ to be proportional to $\exp \lambda \tau$ in Eqs. (33) and (34) and then treat the remaining τ -dependence as being parametric. Thus we have solved the system,

$$\Psi'' - 4\tau^2 k^2 \Psi = 4\tau^2 k \Theta, \quad (41)$$

$$\Theta'' + 2\eta \Theta' - 4\tau^2 k^2 \Theta - 4\tau^2 k \operatorname{erfc}(\eta) \Psi = 2\tau \lambda \Theta, \quad (42)$$

as an eigenvalue problem for λ , and λ was then maximised over k for chosen values of τ . The resulting curve, like the neutral curve itself, gives merely a good representation of the stability properties of the evolving system. For any chosen value of τ , the corresponding point on this dotted curve represents the wavenumber which takes the largest value of λ . The point at which this curve crosses the neutral curve corresponds to $\lambda = 0$ and is the critical point.

It is quite easy to show analytically that $\lambda = -1/\tau$ when $k = 0$, and therefore cells of sufficiently large aspect ratio are always stable. It is of some interest to see that the zero wavenumber cell has the largest value of λ when $\tau < 1.253314$, even though we have $\lambda < 0$ which implies that the basic state is stable at such an early time. This may be related to the fact that the most unstable mode for the Darcy–Bénard problem with constant heat flux heating corresponds to $k = 0$. A brief derivation of this transitional value of τ is given in Appendix 1.

Figure 1b also shows that the right-hand branch of the neutral curve tends towards $k = 1$ when τ is large. This is rather an unusual behaviour since these branches usually satisfy either $k \rightarrow 0$ or $k \rightarrow \infty$ as $\tau \rightarrow \infty$. This asymptote has been analysed in detail in Appendix 2 and a four-term expression of k in terms of τ is given in Eq. (73). Figure 2 shows a close-up of the neutral curves in (k, τ) -space including curves corresponding to two, three and four terms of the expansion given in Eq. (73). It is clear to see that the fit with the computed curves is remarkably good when four terms are included. Rather unusually, the three-term curve has a poorer match than the two-term curve has, but very small values of τ are being represented in Fig. 2, and the series shown in Eq. (73) have successive terms whose ratios are only of $O(\tau^{-1/3})$, and therefore two- and three-term expansions will provide excellent agreement only at much larger values of τ .

Figure 2 also shows a one-term small- k analysis of the neutral curve. The numerical data suggested that $k\tau^2$ is roughly constant when $\tau \gg 1$, and it is straightforward to show that a one-term representation of the neutral curve is,

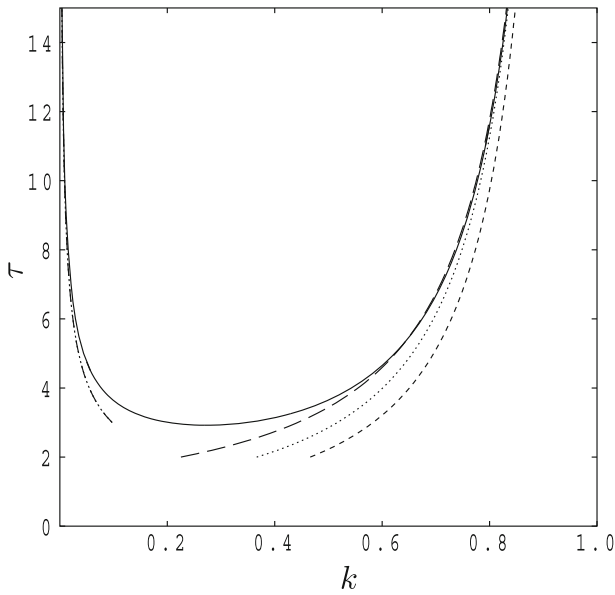


Fig. 2 Neutral curve showing the variation of τ with k together with the asymptotic representation for both small values of k and values close to 1. The *dashed-dotted line* corresponds to $k \ll 1$. For $k \sim 1$: two terms (*dotted*); three terms (*short dashes*); four terms (*long dashes*).

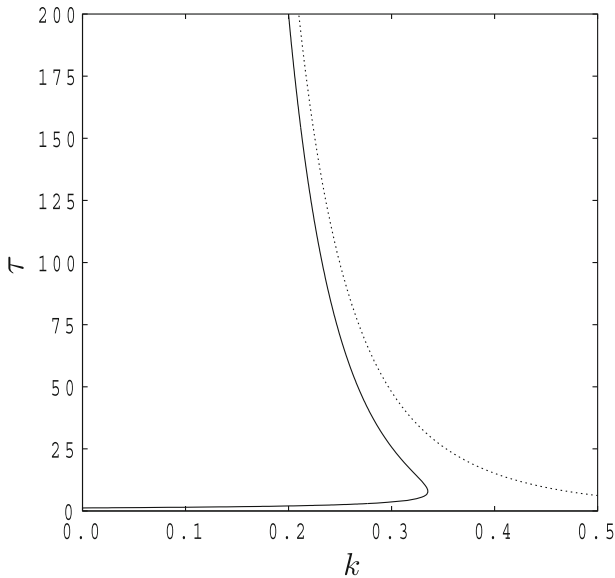


Fig. 3 The location of the wavenumber corresponding to the fastest growth rate of disturbances: numerical data (*continuous line*), asymptotic data (*dotted line*)

$$k \sim \frac{0.8766263}{\tau^2}, \tag{43}$$

where all the displayed significant figures are correct.

An analysis of the fastest growing mode has been undertaken and is given in detail in Appendix 3. It is shown there that the fastest growing mode arises when,

$$k \sim 0.789332\tau^{-1/4}, \quad (44)$$

which is a very slow decay as τ increases. A comparison with our numerical data up to $\tau = 200$ is shown in Fig. 3. It is found that agreement between the numerical data and a one-term asymptotic formula is quite good.

5.2 Comment

For this type of approximation considered in this subsection, neutrality corresponds to when every single point of the θ -profile achieves its minimum value as either τ or t increases since the neutral curves correspond to $\Theta_\tau = 0$. This is a constraint on the system and it will have the effect of yielding later onset times than those obtained without such a constraint. A solution of the full parabolic system allows the temperature profile to evolve freely subject to no constraint other than the boundary conditions. Therefore it is an *a priori* expectation that the parabolic simulation should yield instability at earlier times than that given by an analysis based on a QSSA.

5.3 Parabolic Simulations

The rest of the present paper is devoted to the presentation of solutions of the full linearised disturbance Eqs. (33) and (34) and a discussion of their significance. Stability characteristics inferred from these solutions will also be compared with the quasi-steady stability analysis shown in Fig. 1.

Parabolic simulations of the system given by Eqs. (33) and (34) were undertaken using the Keller-box method. A considerable amount of care was needed to be taken to ensure that reliable solutions were obtained. Three different codes were used which employed the following types of discretisation in the τ -direction: (a) standard second-order central differences, (b) first-order backward differences, (c) second-order backward differences (the so-called BDF2 method). For code-(a) it was found that solutions are subject to pointwise oscillations in the streamfunction when k is close to 1 even when the steplength in τ is as small as 0.01. The greatly improved numerical stability properties of code-(b) removed completely the pointwise oscillations but this is at the expense of accuracy. In addition, this method over-estimates the critical value of τ when k gets close to 1. Code-(c) regains second-order accuracy without pointwise oscillations, and yields reliable onset data when $k \rightarrow 1$. Therefore we adopted the BDF2 method for discretisation in the τ -direction. The steplength in the τ -direction was 0.01.

Central differences and a uniform grid were used in the η -direction with $\eta_{\max} = 3$ and 600 intervals. Although this value of η_{\max} contains the evolving boundary layer well when k is relatively large, it is too small when k takes smaller values. The presence of the term $2\eta\Theta'$ in Eq. (42) guarantees super-exponential decay in Θ , a decay which is essentially complete when $\eta = 2$. On the other hand, Eq. (41) shows that the large- η behaviour of Ψ is that it is proportional to $e^{(-2\tau k)\eta}$ and it therefore has an e-folding distance of $1/(2\tau k)$. This exponential decay may be guaranteed on a small computational domain by replacing the boundary condition, $\Psi = 0$, at $\eta = \eta_{\max}$, by the following,

$$\Psi' + 2\tau k\Psi = 0. \tag{45}$$

As our aim here is to study the stability characteristics of the thermal boundary layer after introducing thermal disturbances, we are interested in the manner in which the cells evolve in time as a function of the initiation time of the disturbance, its initial spanwise profile and its wavenumber. The standard disturbance profile was taken to be, $\Theta = e^{-\eta^2}$, which is introduced at $\tau = \tau_0$ for different values of τ_0 . In turn we shall alter the profiles, the wavenumbers and initiation times in order to gain a comprehensive picture of the stability characteristics of the developing thermal field.

The status of the evolving disturbances (i.e., whether they are decaying or growing) was monitored by the computation of the following quantities: (i) the surface temperature, (ii) a functional based on Θ^2 . We will therefore define the following three quantities,

$$A_1 = \Theta(0), \quad A_2 = \sqrt{\frac{1}{2} \int_0^\infty \Theta^2 dy} = \sqrt{\tau \int_0^\infty \Theta^2 d\eta}. \tag{46}$$

In all cases, we found that amplitude measures decay at first and eventually grow as τ increases whenever $k < 1$, otherwise they always decay with time. Neutrality will then correspond to when these quantities reach their minimum values. The minima we will plot were obtained by detecting the smallest value of the datasets for each A_j -value, followed by fitting a quadratic through that point and the two immediately before and after it, and determining the minimum of the quadratic. This process yields very smooth neutral curves.

Figure 4 shows a comparison of the QSSA neutral curve with those which are obtained from the parabolic simulations and which correspond to the amplitude measures, A_1 and A_2 . Curiously, the surface temperature measure, A_1 , mimics very closely the QSSA neutral curve along the whole of its length. The A_2 curve shows an earlier onset time than that given by the QSSA analysis, and the numerical data gives the following location for the minimum in the neutral curve:

$$\tau_c = 2.5154, \quad k_c = 0.2558. \tag{47}$$

These data correspond to when the disturbance, $\Theta = e^{-\eta^2}$, is introduced at $\tau = 0.1$. Previous papers [Rees (2001); Selim and Rees (2007a); Nouri-Borujerdi et al. (2007); Rees et al. (2008)] have sought to determine the effects of varying the time (or location, as appropriate) at which the disturbance is introduced into the boundary layer. Apart from the near-vertical plume which was considered by Rees et al. (2008), all the others which have been quoted found that there is a chosen evolutionary path which the disturbance takes, and the initiating disturbance evolves quickly towards that path. Thus the onset criterion is effectively independent of the time, τ_0 , at which the disturbance is introduced unless τ_0 is too close to the critical value for the current wavenumber. The present convection problem shares these properties; for example, we find the critical values of τ vary only in the fourth significant figure when $k \simeq 0.25$ and τ_0 takes any value below 1.5.

The four above-quoted papers also present information on how the critical data vary with changes in the disturbance profile. Given that $\Theta = e^{-\eta^2}$ is the ‘natural’ profile for disturbances to take at early times (i.e., this profile represents the leading-order small- τ disturbance shape in an analysis which is similar in style to that contained in Appendix 1), it might be thought it represents a special case where the disturbance is already very close to that forming the favoured evolutionary path and it might be considered that this is the

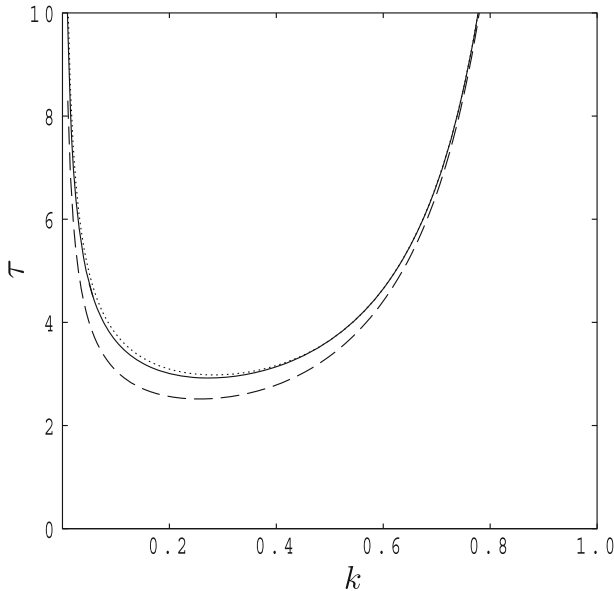


Fig. 4 The three neutral curves corresponding to the QSSA (*continuous line*), the surface temperature, A_1 , (*dotted line*) and the temperature functional, A_2 (*dashed line*).

reason that onset criteria are essentially independent of τ_0 . Therefore we have also undertaken some numerical experiments with disturbances of the form, $\Theta = e^{-c^2\eta^2}$, where $c = 4, 2, 0.5$ and 0.25 . We find that the neutral curve remains virtually unaffected by these thinner and thicker disturbance profiles. Therefore we conclude that the shape of the disturbance is unimportant if it is introduced sufficiently well before the onset times presented above.

Finally, Figure 5 shows how the temperature disturbance profiles vary as time progresses. For ease of presentation, all the profiles have been normalised so that $\Theta = 1$ at $\eta = 0$; in practice the amplitudes decay at first before growing once more. We display such variations in the profile for $k = 0.05, 0.3$ and 0.9 . In all cases, the original $e^{-\eta^2}$ shape evolves towards one where the maximum temperature of the profile is within the porous medium rather at the $\eta = 0$ boundary. As time progresses, the thickness of the profile decreases (in terms of η) and the disturbance becomes increasingly concentrated towards the boundary. This process occurs more quickly for larger values of k .

Although Appendix 2 is concerned with the $k \sim 1$ asymptote in the QSSA neutral curve, the boundary layer scalings presented there are applicable to large times when k is fixed even for the parabolic simulations. In Eq. (59) we see that the disturbance profile eventually occupies a region with the thickness, $\eta = O(\tau^{-2/3})$ when τ is large. This means that disturbance occupies a region of thickness, $y = O(\tau^{1/3})$, and therefore it continues to grow in thickness in terms of physical space. Appendix 2 also discusses an inner layer within the main disturbance layer; this has thickness, $\eta = O(\tau^{-1})$, and therefore $y = O(1)$. The formation of this inner layer may be seen most clearly in Fig. 5 in the $k = 0.9$ frame as τ increases. The region between $\eta = 0$ and the maximum in the profile is essentially the inner layer in the analysis of Appendix 2.

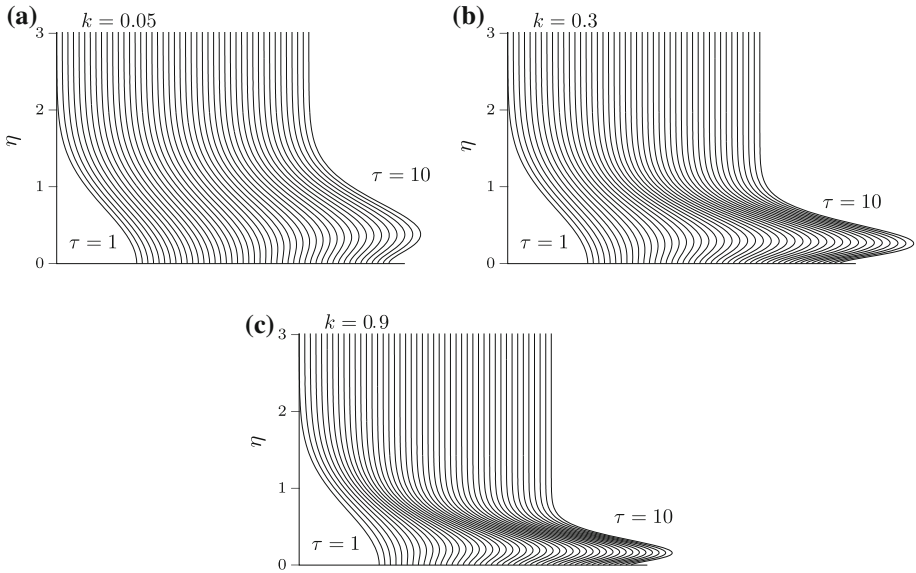


Fig. 5 Displaying the changing shape of the temperature profiles as τ increases from $\tau = 1$ to $\tau = 10$. For $k = 0.05, 0.3$ and 0.9 .

Table 1 Comparison of the onset criteria for the methods of analysis used in this paper and the data given in [Kim et al. \(2004\)](#)

	τ_c	t_c	k_c	$k_c \tau_c$
Local Ra	2.60	6.78	0.45	1.17
QSSA	2.922192	8.538205	0.272965	0.797656
Kim et al. (2004)	2.92	8.54	0.27	0.80
A_1	2.9826	9.8959	0.2837	0.8462
A_2	2.5154	6.3272	0.2558	0.6434

6 Conclusions

In this paper, we have sought to understand the stability characteristics of the conductive thermal boundary layer which arises above a heated horizontal surface in a porous medium. The evolving boundary layer is induced by a constant heat flux which is imposed suddenly at $t = 0$. The onset of convection has been assessed in three different ways, namely a local Rayleigh number analysis, a quasi-static (or frozen time) analysis and a parabolic simulation of the full linearised disturbance equations. In the parabolic simulations we also considered the effect of different initiation times and disturbance profiles, but almost no change in the onset criteria was found provided the disturbance is introduced sufficiently well before the onset time.

We may summarise the onset data in [Table 1](#).

The local Rayleigh number method provides a surprisingly accurate critical time given that it is based on a crude method of comparison between two slightly-related configurations. The predicted wavenumber, though, is reassuringly inaccurate but it is nevertheless well within an order of magnitude of our computations.

Good comparisons are obtained between our QSSA computations and those of [Kim et al. \(2004\)](#), and these are quite close to those obtained by our parabolic simulations using A_1 as a measure of the amplitude of the evolving disturbance. Measured in terms of time, rather than τ , the A_2 amplitude measure yields an onset time which is about 64 % of that corresponding to A_1 . This is quite a significantly early time. The corresponding critical wavenumbers are close.

There are a wide variety of other amplitude measures which could be applied to configurations with an unsteady but nonperiodic basic state. Some of these have been discussed in papers which have already been quoted and involve energy analyses and/or use of Lagrange multipliers to optimise disturbance shapes. But such methods also have multiple ways in which the optimisation constraint may be defined.

Acknowledgements The authors would like to thank the reviewers for their useful comments.

Appendix 1: Small- k Analysis for the Fastest Growing Mode

In this Appendix we solve Eqs. (41) and (42) for small values of k in order to determine that value of τ below which $k = 0$ corresponds to the maximal value of λ . We introduce the following expansions,

$$\Psi = k\Psi_0(\eta) + k^3\Psi_1(\eta) + \dots, \tag{48}$$

$$\Theta = \Theta_0(\eta) + k^2\Theta_1(\eta) + \dots, \tag{49}$$

and

$$\lambda = \lambda_0 + k^2\lambda_1 + \dots. \tag{50}$$

At leading order Θ_0 satisfies,

$$\Theta_0'' + 2\eta\Theta_0' = 2\tau\lambda_0\Theta_0, \tag{51}$$

for which a suitable solution is

$$\Theta_0 = e^{-\eta^2}, \tag{52}$$

where $\lambda_0 = -1/\tau$. This shows that the $k = 0$ mode is always stable. The corresponding equation for Ψ_0 is

$$\Psi_0'' = 4\tau^2e^{-\eta^2}, \tag{53}$$

and its solution is,

$$\Psi_0 = 2\tau^2 \left[e^{-\eta^2} - 1 - \sqrt{\pi} \eta \operatorname{erfc}(\eta) \right]. \tag{54}$$

Although this expression for Ψ_0 satisfies $\Psi_0 = 0$ at $\eta = 0$, it does not vanish as $\eta \rightarrow \infty$. However, an outer $\eta = O(k^{-1})$ layer may be evoked which will cause Ψ_0 to decrease exponentially to zero over that lengthscale.

At the next order we have,

$$\Theta_1'' + 2\eta\Theta_1' + 2\Theta_1 = \left[4\tau^2 + 2\tau\lambda_1 \right] e^{-\eta^2} + 8\tau^4 \left[e^{-\eta^2} - 1 - \sqrt{\pi} \eta \operatorname{erfc}(\eta) \right] \operatorname{erfc}(\eta). \tag{55}$$

A straightforward solution using a fourth order Runge–Kutta scheme shows that $\lambda_1 = 0$ when $\tau = 1.253314$. When τ takes larger values then λ_1 is positive, showing that $k = 0$ is

a local minimum for the growth rate. When τ takes smaller values then λ_1 is negative and therefore $k = 0$ is a local maximum for the growth rate, as shown in Fig. 1.

Appendix 2: Asymptotic Theory for the Right-Hand Branch

In this Appendix we develop an asymptotic expression for the neutral curve as it approaches $k = 1$ with $\tau \gg 1$. We begin with Eqs. (36) and (37) which are repeated below for the sake of completeness,

$$\Psi'' - 4\tau^2 k^2 \Psi = 4\tau^2 k \Theta, \tag{56}$$

$$\Theta'' + 2\eta \Theta' - 4\tau^2 k^2 \Theta - 4\tau^2 k \operatorname{erfc}(\eta) \Psi = 0, \tag{57}$$

and it is recalled that this system needs to be solved subject to $\psi, \theta \rightarrow 0$ as $\eta \rightarrow \infty$ and $\theta' = \psi = 0$ at $\eta = 0$. The detailed numerical results indicate that the right-hand branch approaches the value $k = 1$ as τ increases and that the corresponding eigenfunctions occupy a thinning region in terms of η . Under the assumption that $\tau \gg 1$, it turns out that k expands in inverse powers of τ with

$$k = 1 + k_0 \tau^{-2/3} + k_1 \tau^{-1} + k_2 \tau^{-4/3} + \dots \tag{58}$$

In what follows we evaluate k_0, k_1 and k_2 and remark that we anticipate that $k_0 < 0$ since the neutral curve approaches the $k = 1$ asymptote from the left.

The Main Disturbance Layer

The disturbance is confined to a relatively thin region wherein the appropriate vertical variable is

$$\zeta = \eta \tau^{2/3} = O(1), \tag{59}$$

and for which the error function which appears in Eq. (57) becomes

$$\operatorname{erfc}(\eta) = 1 - \frac{2\zeta}{\sqrt{\pi}} \tau^{-2/3} + O(\tau^{-4/3}). \tag{60}$$

Eigensolutions are sought of the form where

$$(\psi, \theta) = (\psi_0, \theta_0) + \tau^{-1/3}(\psi_1, \theta_1) + \tau^{-2/3}(\psi_2, \theta_2) + \tau^{-1}(\psi_3, \theta_3) + \tau^{-4/3}(\psi_4, \theta_4) + \dots, \tag{61}$$

and the substitution of Eqs. (58), (59) and (61) into Eqs. (56) and (57) yields a sequence of equations for (ψ_j, θ_j) .

At both leading (zeroth) and first orders, the streamfunction and heat transport equations are consistent and simply give

$$\psi_0 = -\theta_0 \quad \text{and} \quad \psi_1 = -\theta_1. \tag{62}$$

To tie down these functions, we proceed to higher orders and, at $O(\tau^{4/3})$, Eqs. (56) and (57) give

$$4(\theta_2 + \psi_2) = \psi_0'' - 8k_0 \psi_0 - 4k_0 \theta_0, \tag{63}$$

and

$$4(\psi_2 + \theta_2) = \theta_0'' - 8k_0\theta_0 - 4k_0\psi_0 + \frac{8}{\sqrt{\pi}}\zeta\psi_0, \quad (64)$$

where a prime denotes differentiation with respect to ζ here. This pair then yields,

$$\frac{d^2\psi_0}{d\zeta^2} - 4k_0\psi_0 - \frac{4\zeta}{\sqrt{\pi}}\psi_0 = 0, \quad (65)$$

which is a scaled form of Airy's equation with solution

$$\psi_0 = -\theta_0 = CAi \left[\frac{4^{1/3}}{\pi^{1/6}} (\zeta + k_0\sqrt{\pi}) \right], \quad (66)$$

where C is an arbitrary constant.

It is clear that Eq. (66) satisfies $\psi_0, \theta_0 \rightarrow 0$ as $\zeta \rightarrow \infty$, but it does not fulfil the requirements at $\zeta = 0$, namely that $\theta' = \psi = 0$. This points to the existence of an inner sublayer within the disturbance layer, which we analyse below, but here we can impose one of the two wall conditions and make the usual choice to enforce the Dirichlet condition $\psi_0 = 0$. If we denote the first zero of the Airy function as $Z_0 (= -2.338107$ to six decimal places), then Eq. (66) implies that

$$(4\pi)^{1/3}k_0 = Z_0 \Rightarrow k_0 = Z_0/(4\pi)^{1/3}. \quad (67)$$

In order to derive further terms in the asymptotic expansion Eq. (58) it is necessary to consider the governing equations for θ_3 and ψ_3 and for θ_4 and ψ_4 . The consistency of the pair of equations at $O(\tau)$ for θ_3 and ψ_3 is guaranteed as long as

$$\theta_1 = k_1\sqrt{\pi}\frac{d\theta_0}{d\zeta} \quad (68)$$

with ψ_1 then given by Eq. (62). At $O(\tau^{2/3})$ we find that

$$4(\psi_4 + \theta_4) = \psi_2'' - 8k_0\psi_2 - 4k_0\theta_2 - 8k_1\psi_1 - 4k_1\theta_1 - 4(2k_2 + k_0^2)\psi_0 - 4k_2\theta_0$$

and

$$4(\psi_4 + \theta_4) = \theta_2'' - 8k_0\theta_2 - 4k_0\psi_2 + \frac{8}{\sqrt{\pi}}\zeta\psi_2 - 8k_1\theta_1 - 4k_1\psi_1 - 4(2k_2 + k_0^2)\theta_0 - 4k_2\psi_0 + \frac{8k_0\zeta}{\sqrt{\pi}}\psi_0.$$

The solvability of this pair of equations leads to the governing equation for ψ_2 in the form,

$$\frac{d^2\psi_2}{d\zeta^2} - 4k_0\psi_2 - \frac{4\zeta}{\sqrt{\pi}}\psi_2 = \frac{1}{8}\psi_0'''' + 4k_1^2\sqrt{\pi}\psi_0' + 2(k_0^2 + 2k_2)\psi_0, \quad (69)$$

and this can be solved explicitly by making use of the fact that ψ_0 satisfies Eq. (65). It follows that

$$\psi_2 = \frac{\sqrt{\pi}}{160}\psi_0^V + \frac{k_1^2\pi}{2}\psi_0'' + \frac{1}{2}\sqrt{\pi}(k_0^2 + 2k_2)\psi_0';$$

if we denote $\psi_0'(\zeta = 0) = D$ then it can be shown that

$$\psi_2 \rightarrow D \left[\frac{k_0^2\sqrt{\pi}}{10} + \frac{\sqrt{\pi}(k_0^2 + 2k_2)}{2} \right]$$

as $\zeta \rightarrow 0$. Then Eq. (64) implies that

$$\theta_2 \rightarrow \left[\frac{k_0^2 \sqrt{\pi}}{10} + \frac{\sqrt{\pi}(k_0^2 + 2k_2)}{2} \right] \frac{d\theta_0}{d\zeta} \equiv M \frac{d\theta_0}{d\zeta} \tag{70}$$

in this limit. Taken together, Eqs. (66), (68) and (70) show that

$$\theta = \text{Ai} \left[\frac{4^{1/3}}{\pi^{1/6}} (\zeta + k_0 \sqrt{\pi}) \right] + k_1 \sqrt{\pi} \frac{d\theta_0}{d\zeta} \tau^{1/3} + M \frac{d\theta_0}{d\zeta} \tau^{2/3} + \dots \quad \text{as } \zeta \rightarrow 0,$$

and it is therefore necessary to consider the sub-layer in order to satisfy the Neumann boundary condition on θ at $\eta = 0$.

The Sublayer

Within the sublayer, where $\zeta = \tau^{-1/3} \hat{\eta}$, the main layer solutions imply that,

$$\theta = \tau^{-1/3} \hat{\theta}_0(\hat{\eta}) + \tau^{-2/3} \hat{\theta}_1(\hat{\eta}) + \dots, \quad \psi = \tau^{-1/3} \hat{\psi}_0(\hat{\eta}) + \tau^{-2/3} \hat{\psi}_1(\hat{\eta}) + \dots.$$

Substituting gives at the first two orders

$$\hat{\psi}_j'' - 4\hat{\psi}_j = 4\hat{\theta}_j \quad \text{and} \quad \hat{\theta}_j'' - 4\hat{\theta}_j = 4\hat{\psi}_j \quad (j = 0, 1),$$

whereupon

$$\hat{\theta}_0 = \lambda \left[e^{-\sqrt{8}\hat{\eta}} + 1 + \hat{\eta}\sqrt{8} \right], \quad \hat{\psi}_0 = \lambda \left[e^{-\sqrt{8}\hat{\eta}} - 1 - \hat{\eta}\sqrt{8} \right],$$

for some constant λ that can be determined by matching but whose precise value is not required here. These leading order solutions are only compatible with the main layer structure if

$$k_1 \sqrt{\pi} = \frac{1}{\sqrt{8}}. \tag{71}$$

The equations for $\hat{\theta}_1$ and $\hat{\psi}_1$ need to be solved such that both $\hat{\theta}'_1$ and $\hat{\psi}'_1$ vanish on the wall and tend to constants as $\hat{\eta} \rightarrow \infty$. The only way this is possible is if the constant is zero and then these functions are both identically zero. We deduce that

$$M = \frac{k_0^2 \sqrt{\pi}}{10} + \frac{\sqrt{\pi}(k_0^2 + 2k_2)}{2} = 0 \quad \Rightarrow \quad k_2 = -\frac{3k_0^2}{5}. \tag{72}$$

Combining results of Eqs. (67), (71) and (72) yields the shape of the neutral curve for large τ in the form,

$$\begin{aligned} k &= 1 + \frac{Z_0(4\pi)^{-1/3}}{\tau^{2/3}} + \frac{1}{\sqrt{8\pi}\tau} - \frac{0.6Z_0^2(4\pi)^{-2/3}}{\tau^{4/3}} + \dots \\ &\approx 1 - 1.006\tau^{-2/3} + 0.199\tau^{-1} - 0.607\tau^{-4/3} + \dots, \end{aligned} \tag{73}$$

where $Z_0 = -2.338107$ was used in the computations depicted in Fig. 2.

Appendix 3: Asymptotic Form of the Fastest Growing Mode When $\tau \gg 1$

Here we outline the structure of the fastest growing mode for large scaled times. For completeness, it is convenient to start with the relevant system,

$$\Psi'' - 4\tau^2 k^2 \Psi = 4\tau^2 k \Theta, \tag{74}$$

$$\Theta'' + 2\eta \Theta' - 4\tau^2 k^2 \Theta - 4\tau^2 k \operatorname{erfc}(\eta) \Psi = 2\tau \lambda \Theta, \tag{75}$$

which one may recall is the eigenvalue problem for λ , but where λ is to be maximised over k for chosen values of τ .

To infer the structure of the desired mode it is easiest to consider the form of solution of the problem for a general value of $k = O(1)$ and then allow $k \rightarrow 0$. Doing this leads to the conclusion that the most dangerous mode resides in the regime where $k = O(\tau^{-1/4})$ and it is compressed into a thin zone attached to $\eta = 0$ and of depth $O(\tau^{-1/2})$. In brief, the spatial variable is then

$$\tilde{\zeta} = \eta \tau^{1/2} = O(1), \tag{76}$$

the growth rate

$$\lambda = 2\tau + \lambda_0 \tau^{1/2} + \dots, \tag{77}$$

the wavenumber of interest is

$$k = \mathcal{K} \tau^{-1/4} + \dots \tag{78}$$

and eigensolutions are sought of the form

$$\psi = \tilde{\psi}_0 + \tau^{-1/4} \tilde{\psi}_1 + \tau^{-1/4} \tilde{\psi}_2 + \dots \quad \theta = \tau^{-1/4} \tilde{\theta}_0 + \tau^{-1/2} \tilde{\theta}_1 + \tau^{-1/2} \tilde{\theta}_2 + \dots \tag{79}$$

At both leading and first orders, the streamfunction and heat transport equations are consistent and simply give

$$\mathcal{K} \tilde{\psi}_0 = -\tilde{\theta}_0 \quad \text{and} \quad \mathcal{K} \tilde{\psi}_1 = -\tilde{\theta}_1. \tag{80}$$

Consistency at next order is only possible if

$$\frac{d^2 \tilde{\theta}_0}{d\zeta^2} - \left[\frac{8\mathcal{K}^2}{\sqrt{\pi}} \zeta + 4\mathcal{K}^2 \left(\mathcal{K}^2 + \frac{1}{2} \lambda_0 \right) \right] \tilde{\theta}_0 = 0. \tag{81}$$

Much as in the case of discussion of the problem Eq. (65), the requirement that this equation possesses a solution with decay both as $\tilde{\zeta} \rightarrow 0$ and as $\tilde{\zeta} \rightarrow \infty$ requires that

$$\lambda_0 = \frac{2Z_0}{\pi^{1/3}} \mathcal{K}^{-2/3} - 2\mathcal{K}^2, \tag{82}$$

where Z_0 is the first zero of the Airy function.

It is now evident how the analysis has captured the fastest growing mode. The expression Eq. (82) for $\lambda_0 \rightarrow -\infty$ both as $\mathcal{K} \rightarrow 0$ and $\mathcal{K} \rightarrow \infty$; it is a simple matter to show that λ_0 is maximised when $\mathcal{K} \approx 0.789332$ and hence we deduce the quoted result Eq. (44). There is good agreement between this analytical prediction and the numerical simulations—this comparison could be improved by including higher order terms in our analysis although the algebraic manipulations very rapidly become increasingly laborious. But this Appendix illustrates how that the wavenumber of the fastest growing mode decreases slowly with τ .

References

- Caltagirone, J.-P.: Stability of a saturated porous layer subject to a sudden rise in surface temperature: comparison between the linear and energy methods. *Quart. J. Mech. Appl. Math.* **33**, 47–58 (1980)
- Carslaw, H.S., Jaeger, J.C.: *Conduction of Heat in Solids*, 2nd edn. Clarendon Press, Oxford (1959)
- Elder, J.W.: Transient convection in a porous medium. *J. Fluid Mech.* **27**, 609–623 (1967)
- Elder, J.W.: The unstable thermal interface. *J. Fluid Mech.* **32**, 69–96 (1968)
- Ennis-King, J.P., Paterson, L.: Coupling of geochemical reactions and convective mixing in the long-term geological storage of carbon dioxide. *Int. J. Greenhouse Gas Control* **1**, 86–93 (2007)
- Hassanzadeh, H., Pooladi-Darvish, M., Keith, D.W.: Scaling behavior of convective mixing, with application to geological storage of CO₂. *AIChE J.* **53**, 1121–1131 (2007)
- Hassanzadeh, H., Pooladi-Darvish, M., Keith, D.W.: The effect of natural flow of aquifers and associated dispersion on the onset of buoyancy-driven convection in a saturated porous medium. *AIChE J.* **55**, 475–485 (2009)
- Hidalgo, J.J., Carrera, J.: Effect of dispersion on the onset of convection during CO₂ sequestration. *J. Fluid Mech.* **640**, 441–452 (2009)
- Hong, J.S., Kim, M.N., Yoon, D.-Y., Chung, B.-J., Kim, M.C.: Linear stability analysis of a fluid-saturated porous layer subjected to time-dependent heating. *Int. J. Heat Mass Transfer* **51**, 3044–3051 (2008)
- Keller, H.B., Cebeci, T.: Accurate numerical methods for boundary layer flows 1. Two dimensional flows. *Proceedings International Conference Numerical Methods in Fluid Dynamics, Lecture Notes in Physics*. Springer, New York (1971)
- Kim, M.C., Kim, S., Choi, C.K.: Convective instability in fluid-saturated porous layer under uniform volumetric heat sources. *Int. Comm. Heat Mass Transfer* **29**, 919–928 (2002)
- Kim, M.C., Kim, K.Y., Kim, S.: The onset of transient convection in fluid-saturated porous layer heated uniformly from below. *Int. Comm. Heat Mass Transfer* **31**, 53–62 (2004)
- Kuznetsov, A.V., Nield, D.A., Simmons, C.T.: The onset of convection in a strongly heterogeneous porous medium with transient temperature profile. *Transp. Porous Med.* **86**, 851–865 (2011)
- Nield, D.A., Bejan, A.: *Convection in Porous Media*, 3rd edn. Springer, New York (2006)
- Nield, D.A., Kuznetsov, A.V.: The onset of convection in a heterogeneous porous medium with transient temperature profile. *Transp. Porous Med.* **85**, 691–702 (2010)
- Nouri-Borujerdi, A., Nogrehabadi, A.R., Rees, D.A.S.: The linear stability of a developing thermal front in a porous medium: the effect of local thermal nonequilibrium. *Int. J. Heat Mass Transfer* **50**, 3090–3099 (2007)
- Rapaka, S., Chen, S., Pawar, R., Stauffer, P.H., Zhang, D.: Non-modal growth of perturbations in density-driven convection in porous media. *J. Fluid Mech.* **609**, 285–303 (2008)
- Rees, D.A.S.: Vortex instability from a near-vertical heated surface in a porous medium. I. Linear theory. *Proc. R. Soc. A* **457**, 1721–1734 (2001)
- Rees, D.A.S., Postelnicu, A., Bassom, A.P.: The linear vortex instability of the near-vertical line source plume in porous media. *Transp. Porous Med.* **74**, 221–238 (2008a)
- Rees, D.A.S., Selim, A., Ennis-King, J.P.: The instability of unsteady boundary layers in porous media. In: Vadasz, P. (ed.) *Emerging Topics in Heat and Mass Transfer in Porous Media*, pp. 85–110. Springer, New York (2008b)
- Riaz, A., Hesse, M., Tchelepi, H.A., Orr, F.M.: Onset of convection in a gravitationally unstable diffusive boundary layer in porous media. *J. Fluid Mech.* **548**, 87–111 (2006)
- Selim, A., Rees, D.A.S.: The stability of a developing thermal front in a porous medium. I. Linear theory. *J. Porous Med.* **11**, 1–15 (2007a)
- Selim, A., Rees, D.A.S.: The stability of a developing thermal front in a porous medium. II. Nonlinear theory. *J. Porous Med.* **11**, 17–33 (2007b)
- Selim, A., Rees, D.A.S.: The stability of a developing thermal front in a porous medium. III. Secondary instabilities. *J. Porous Med.* **13**, 1039–1058 (2010a)
- Selim, A., Rees, D.A.S.: Linear and nonlinear evolution of isolated disturbances in a growing thermal boundary layer in porous media. *Third International Conference on Porous Media and its Applications in Science, Engineering and Industry June 20–25 2010, Montecatini, Italy. AIP Conference Proceedings*, Vol. 1254, pp. 47–52 (2010b).
- Tan, K.-K., Sam, T., Jamaludin, H.: The onset of transient convection in bottom heated porous media. *Int. J. Heat Mass Transfer* **46**, 2857–2873 (2003)
- Wessel-Berg, D.: On a linear stability problem related to underground CO₂ storage. *SIAM J. Appl. Math.* **70**, 1219–1238 (2009)
- Yoon, D.Y., Choi, C.K.: Thermal convection in a saturated porous medium subjected to isothermal heating. *Korean J. Chem. Eng.* **6**, 144–149 (1989)